Investigation of Nozzle Flow and Cavitation Characteristics in a Diesel Injector

S. Som[1]
e-mail: ssom1@uic.edu

S. K. Aggarwal

Department of Mechanical and Industrial Engineering,
University of Illinois at Chicago,
842 West Taylor Street,
Chicago, IL 60607-7022

E. M. El-Hannouny

D. E. Longman

Center for Transportation Research,
Argonne National Laboratory,
Argonne, IL 60439

Cavitation and turbulence inside a diesel injector play a critical role in primary spray breakup and development processes. The study of cavitation in realistic injectors is challenging, both theoretically and experimentally, since the associated two-phase flow field is turbulent and highly complex, characterized by large pressure gradients and small orifice geometries. We report herein a computational investigation of the internal nozzle flow and cavitation characteristics in a diesel injector. A mixture based model in FLUENT V6.2 software is employed for simulations. In addition, a new criterion for cavitation inception based on the total stress is implemented, and its effectiveness in predicting cavitation is evaluated. Results indicate that under realistic diesel engine conditions, cavitation patterns inside the orifice are influenced by the new cavitation criterion. Simulations are validated using the available two-phase nozzle flow data and the rate of injection measurements at various injection pressures (800–1600 bar) from the present study. The computational model is then used to characterize the effects of important injector parameters on the internal nozzle flow and cavitation behavior, as well as on flow properties at the nozzle exit. The parameters include injection pressure, needle lift position, and fuel type. The propensity of cavitation for different on-fleet diesel fuels is compared with that for n-dodecane, a diesel fuel surrogate. Results indicate that the cavitation characteristics of n-dodecane are significantly different from those of the other three fuels investigated. The effect of needle movement on cavitation is investigated by performing simulations at different needle lift positions. Cavitation patterns are seen to shift dramatically as the needle lift position is changed during an injection event. The region of significant cavitation shifts from top of the orifice to bottom of the orifice as the needle position is changed from fully open (0.275 mm) to nearly closed (0.1 mm), and this behavior can be attributed to the effect of needle position on flow patterns upstream of the orifice. The results demonstrate the capability of the cavitation model to predict cavitating nozzle flows in realistic diesel injectors and provide boundary conditions, in terms of vapor fraction, velocity, and turbulence parameters at the nozzle exit, which can be coupled with the primary breakup simulation. [DOI: 10.1115/1.3203146]

1 Introduction

Cavitation refers to the formation of bubbles in a liquid flow leading to a two-phase mixture of liquid and vapor/gas, when the local pressure drops below the vapor pressure of the fluid. Fundamentally, the liquid to vapor transition can occur by heating the fluid at a constant pressure, known as boiling, or by decreasing the pressure at a constant temperature, which is known as cavitation. Since vapor density is at least two orders of magnitudes smaller than that of liquid, the phase transition is assumed to be an isothermal process. Cavitation has also been defined as "the liquid continuum rupture due to excessive stress" by Franc et al. [1]. For most applications, cavitation is hypothesized to occur as soon as the local pressure drops below the vapor pressure of the fluid at the specified temperature. Modern diesel engines are designed to operate at elevated injection pressures corresponding to high injection velocities. Therefore, in a diesel injector nozzle, high-pressure gradients and shear stresses can lead to cavitation or to the formation of bubbles.

Cavitation is commonly encountered in hydrodynamic equipment, such as pumps, valves, etc., where it is not desirable since it can severely affect the system efficiency, cause mechanical wear, and potentially damage the equipment. In diesel fuel injectors, cavitation can be beneficial to the development of the fuel spray, since the primary break-up and subsequent atomization of the liquid fuel jet can be enhanced. Primary breakup is believed to occur in the region very close to the nozzle tip as a result of turbulence, aerodynamics, and inherent instability caused by the cavitation patterns inside the injector nozzle orifices. In addition, cavitation increases the liquid velocity at the nozzle exit due to the reduced exit area available for the liquid. Cavitation patterns extend from their starting point around the nozzle orifice inlet to the exit, where they influence the formation of the emerging spray. The improved spray development is believed to lead to a more complete combustion process, lower fuel consumption, and reduced exhaust gas and particulate emissions. However, cavitation can also decrease the flow efficiency (discharge coefficient) due to its affect on the exiting jet. Also imploding cavitation bubbles inside the orifice can cause material erosion thus decreasing the life and performance of the injector. Clearly an optimum amount of cavitation is desirable, and it is important to understand the sources and amount of cavitation for more efficient nozzle designs. Cavitation inception can be caused by "geometrical" and "dynamic" factors [2]. Geometrical parameters include the type of orifice (valve covered orifice (VCO) or minisac), orifice inlet curvature, orifice length, ratio of inlet to outlet orifice diameter, and its surface roughness. Dynamic parameters include the imposed pressure gradient, injector needle lift, and needle eccentricity.

Numerous experimental and computational/modeling investigations have been reported focusing on the initiation of cavitation and the ensuing two-phase flow inside the diesel engine injector. A good review of the various modeling approaches can be found

[1]Corresponding author.

Manuscript received November 13, 2008; final manuscript received April 6, 2009; published online January 15, 2010. Review conducted by Kalyan Annamalai.

in Ref. [3]. As discussed in the cited study, the various cavitation models can essentially be categorized into two groups: (1) single fluid/continuum models and (2) two-fluid models. In single fluid/continuum models, the average mixture properties, such as density and viscosity, are determined based on the vapor volume fraction. Schmidt et al. [4] developed a model in which the liquid and vapor are assumed to be in thermal equilibrium; two phases are uniformly distributed within each cell, and there is no-slip between the liquid and vapor phases. Liquid and vapor phases were considered incompressible, whereas the liquid/vapor mixture was considered compressible. Then, assuming an isentropic flow, a barotropic equation was used for closure, and the two-phase sound speed was modeled using the Wallis approach [5]. The major drawback of this model is that nozzle flows are inherently turbulent and the lack of turbulence consideration removes essential characteristics of the flow. Other studies using this approach include Refs. [6–9].

In two-fluid models, the liquid and vapor phases are treated separately using two sets of conservation equations. The various models here can be grouped into two broad categories, namely, (i) Eulerian–Eulerian models and (ii) Eulerian–Lagrangian models. The Eulerian–Eulerian models are based on the transport of volume fraction, and a source term representing phase transition that is governed by the difference between local pressure and vapor pressure. Cavitation is assumed to occur due to the presence of bubble nuclei or microbubbles within the liquid, which can grow or collapse, as they are convected in the flow, as described by the vapor fraction transport equation. The growth and collapse are taken into account by the Rayleigh's simplified bubble dynamics equation. Studies using this approach have been reported by Chen and Heister [10], Martynov [11], and Singhal et al. [12]. Another approach under this category is that based on the concept of "interpenetrating continua" [13]. In this approach, liquid is treated as a continuous phase and vapor is treated as a as a discrete phase (which is still treated in an Eulerian reference frame), and the two phases are linked to each other using a mass transfer term in mass conservation equation. Bubble dynamics is calculated using a simplified Rayleigh–Plesset equation. Studies using this approach have been reported by Li et al. [9], Tatschl et al. [13], Chiavola and Palmeiri [14], and Dirke et al. [15].

The Eulerian–Lagrangian based models [16] consider liquid as the carrier phase in a Eulerian frame of reference and vapor bubbles as the dispersed phase using a Lagrangian frame of reference. Bubble parcels are used to simulate the entire population of actual bubbles. These parcels are assumed to contain a number of identical noninteracting bubbles. In order to initiate cavitation, nuclei are artificially created, and the size of each nucleus is sampled from a probability density function. Bubble dynamics is calculated using the complete (nonlinear) Rayleigh–Plesset equation. The effect of turbulent dispersion, drag force, pressure gradient, and lift forces on the bubble parcels is also considered. Clearly, this is a more detailed model as it accounts for most dispersed phase processes.

One of the first comprehensive experimental studies on cavitation in diesel injectorlike geometries was performed by Winklhofer et al. [17]. Vapor fraction, static pressure, and velocity field measurements inside the channel were reported. There have also been experimental studies to capture the cavitation phenomenon in scaled-up transparent nozzles [18,19]. Arcoumanis et al. [20] observed that cavitation does not scale up, and therefore actual-size experiments are needed to depict the cavitating flow behavior. Consequently, subsequent studies employed actual-size nozzle orifices. Roth et al. [21] conducted a numerical and experimental study on the effect of multiple injection strategy on cavitation phenomenon, and observed that the cavitation patterns due to the pilot injection are similar to those of the main injection event. Benajes et al. [22] conducted an experimental study to characterize the effect of orifice geometry on the injection rate in a common rail fuel injection system. The major conclusion was that the discharge coefficient was higher in conical nozzles than that in cylindrical nozzles. Badock et al. [23] showed experimentally that increasing the conicity and radii of inlet curvature can reduce cavitation. One of the first studies on the effect of cavitation on spray evolution was performed by Chaves et al. [24], who observed the spray angle to increase with cavitation inception. Payri et al. [25] also observed this behavior, as well as an increase in spray tip penetration with increasing orifice conicity. Han et al. [2] reported an experimental investigation using different multihole minisac and VCO nozzles with cylindrical and tapered geometries, as well as different single-hole nozzles with defined grades of hydrogrinding. While there have been experimental studies dealing with the effect of nozzle orifice geometry on cavitation and subsequent spray development, corresponding theoretical and computational studies have been lacking. Ning et al. [8,26] recently examined the effects of orifice parameters on spray characteristics for a single orifice research nozzle. Simulations qualitatively captured the effects of orifice geometry on spray penetration length, although the spray breakup model only considered the aerodynamic effects. The turbulence and cavitation effects were not included while coupling the nozzle flow model with the spray breakup model.

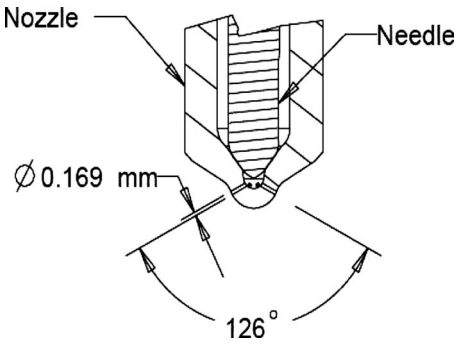

Fig. 1 Schematic of six-hole full-production minisac nozzle. Only two holes are seen in this cross-sectional slice. Nozzle and needle region are identified along with the computational zone used in simulations. The orifice diameter is 169 μm with an included angle of 126 deg.

2 Objectives

The present study has two major objectives. The first is to investigate the internal flow and cavitation phenomena inside a single orifice of a six-hole nozzle, as shown in Fig. 1, and to examine their effects on the nozzle exit flow. Some previous computational studies have examined the nozzle flow and its global effects on spray development [24,25], but have not coupled the flow inside the nozzle to the spray behavior. With the eventual goal of coupling the inner nozzle flow characteristics with the primary jet breakup, as reported in previous studies [27,28], our focus here is to characterize the effects of various parameters on the two-phase flow properties at the nozzle exit. The present study intends to provide turbulence quantities, discharge coefficient, vapor fraction, and velocity distributions at the nozzle exit, which can subsequently be used in modeling primary breakup. Simulations were based on a "full cavitation model" [12,29,30] in FLUENT V6.2 software. First, we performed extensive validation using the available two-phase nozzle flow data, as well as flow efficiency data from our experiments. The computational model was then used to investigate the effects of needle lift and orifice geometry on flow characteristics inside the nozzle, as well as on cavitation and turbulence levels at the nozzle exit. In addition, the effect of fuel type on cavitation was characterized by considering four different fuels.

The second objective is to examine a new criterion for cavitation inception under realistic high-pressure diesel engine condi-

Table 1 Test conditions for rate of injection measurements

Parameter	Quantity
Injection system	Caterpillar HEUI 315B
Oil rail pressure (MPa)	Case 1:17|Case 2:21| Case 3: 24
Ambient gas	Nitrogen (N_2)
Chamber density (kg/m^3)	34.13
Chamber temperature (°C)	30
Fuel	Viscor/cerium blend
Fuel temperature (°C)	40
Fuel injection quantity (mm^3/stroke)	250

tions. This new criterion has been proposed by Joseph [31], and is based on the total stress that includes both the pressure and normal viscous stresses. We have further modified this criterion so that it can be used in both the laminar and turbulent cavitating flows, implemented it in FLUENT, and evaluated its effectiveness to predict cavitation under realistic diesel engine conditions, which include realistic injection pressures and nozzle geometry. We believe this is the first time that this new criterion has been evaluated under such conditions. Our literature review also indicates the dearth of quantitative experimental data for inner nozzle flow validations. Therefore, another objective of the present study was to report rate of injection (ROI) measurements at different injection pressures and discharge coefficients under realistic injection conditions, which may be used by the injector flow modeling community.

3 Computational Model

The commercial computational fluid dynamics (CFD) software FLUENT V6.2 was used to perform the numerical simulation of flow inside the nozzle. FLUENT employs a mixture based model, as proposed by Singhal et al. [12]. The nozzle flow is considered isothermal, which is justified based on previous experimental studies, which indicate that the temperature difference between the fuel inlet and exit is typically not more than 10 K (cf. Table 1). The two-phase model considers a mixture comprising of liquid fuel, vapor, and a noncondensable gas. While the gas is compressible, the liquid and vapor are considered incompressible. The mixture is also modeled as incompressible. In addition, a no-slip condition between the liquid and vapor phases is assumed. Then the mixture properties are computed by using the Reynolds-averaged continuity and momentum equations [29]

$$\frac{\partial u_j}{\partial x_j} = 0 \tag{1}$$

$$\rho \frac{\partial u_i u_j}{\partial x_j} = -\frac{\partial P}{\partial x_i} + \frac{\partial \tau_{ij}}{\partial x_j} \tag{2}$$

where

$$\tau_{ij} = (\mu + \mu_t)\left\{\frac{\partial u_i}{\partial x_j} + \frac{\partial u_j}{\partial x_i}\right\}$$

and

$$\mu_t = C_\mu \rho \left(\frac{k^2}{\in}\right)$$

is the turbulent viscosity.

In order to account for large pressure gradients, the realizable $k-\in$ turbulence model is incorporated along with the nonequilibrium wall functions

$$\frac{\partial \rho u_j k}{\partial x_j} = \frac{\partial}{\partial x_j}\left[\left(\mu + \frac{\mu_t}{\sigma_k}\right)\frac{\partial k}{\partial x_j}\right] + P - \rho \in \tag{3}$$

where the production of turbulent kinetic energy

$$P = \mu_t \frac{\partial u_i}{\partial x_j}\left[\frac{\partial u_i}{\partial x_j} + \frac{\partial u_j}{\partial x_i}\right] - \frac{2}{3}\frac{\partial u_i}{\partial x_i}\left\{\rho k + \mu_t \frac{\partial u_k}{\partial x_k}\right\}$$

$$\frac{\partial \rho u_j \in}{\partial x_j} = \frac{\partial}{\partial x_j}\left[\left(\mu + \frac{\mu_t}{\sigma_k}\right)\frac{\partial \in}{\partial x_j}\right] + \frac{\in}{k}\left[c_1 P - c_2 \rho \in + c_3 \rho k \frac{\partial u_k}{\partial x_k}\right] \tag{4}$$

The turbulent viscosity is modeled for the whole mixture. The mixture density and viscosity are calculated using the following equations:

$$\rho = \alpha_v \rho_v + (1 - \alpha_v - \alpha_g)\rho_l + \alpha_g \rho_g \tag{5}$$

$$\mu = \alpha_v \mu_v + (1 - \alpha_v - \alpha_g)\mu_l + \alpha_g \mu_g \tag{6}$$

where ρ and μ are the mixture density and viscosity, respectively, and the subscripts v, l, and g represent the vapor, liquid, and gas, respectively. The mass (f) and volume fractions (α) are related as

$$\alpha_v = f_v \frac{\rho}{\rho_v}, \quad \alpha_l = f_l \frac{\rho}{\rho_l}, \quad \text{and} \quad \alpha_g = f_g \frac{\rho}{\rho_g} \tag{7}$$

Then the mixture density can be expressed as

$$\frac{1}{\rho} = \frac{f_v}{\rho_v} + \frac{f_g}{\rho_g} + \frac{1 - f_v - f_g}{\rho_l} \tag{8}$$

The vapor transport equation governing the vapor mass fraction is as follows:

$$\rho \frac{\partial u_j f_v}{\partial x_j} = \frac{\partial}{\partial x_j}\left(\Gamma \frac{\partial f_v}{\partial x_j}\right) + R_e - R_c \tag{9}$$

where u_i is the velocity component in a given direction ($i = 1, 2, 3$), Γ is the effective diffusion coefficient, and R_e and R_c are the vapor generation and condensation rate terms [29] computed as

$$R_e = C_e \frac{\sqrt{k}}{\sigma}\rho_l \rho_v (1 - f_v - f_g)\sqrt{\frac{2(P_v - P)}{3\rho_l}}$$

$$R_c = C_c \frac{\sqrt{k}}{\sigma}\rho_l \rho_v f_v \sqrt{\frac{2(P - P_v)}{3\rho_l}} \tag{10}$$

where σ and P_v are the surface tension and vapor pressure of the fluid, respectively, and k and P are the local turbulent kinetic energy and static pressure, respectively. An underlying assumption here is that the phenomenon of cavitation inception (bubble creation) is the same as that of bubble condensation or collapse. Turbulence induced pressure fluctuations are accounted for by changing the phase-change threshold pressure at a specified temperature (P_{sat}) as

$$P_v = P_{sat} + P_{turb}/2 \tag{11}$$

where $P_{turb} = 0.39\rho k$. The source and sink terms in Eq. (10) are obtained from the simplified solution of the Rayleigh–Plesset equation [12,29]. No-slip boundary conditions at the walls and symmetry boundary condition at the center line are employed for the HEUI 315-B injector simulations.

4 Validation of the Computation Model

The experimental data from Ref. [17] was used for a comprehensive model validation. These experiments were conducted in a transparent quasi-two-dimensional geometry, wherein the back pressure was varied to achieve different mass flow rates. To the best of our knowledge this experimental data set is the most comprehensive in terms of two-phase information and inner nozzle flow properties. A rectangular converging channel was used with an inlet width (D_{in}) of 301 μm, outlet width (D_{out}) of 284 μm, length (L) of 1000 μm, inlet rounding radius (r) of 20 μm, and thickness of 300 μm. These dimensions correspond to an $r/R_{in} = 0.133$, $L/D_{in} = 3.322$, and $K_{factor} = 1.7$ (cf. Eq. 29), which are rep-

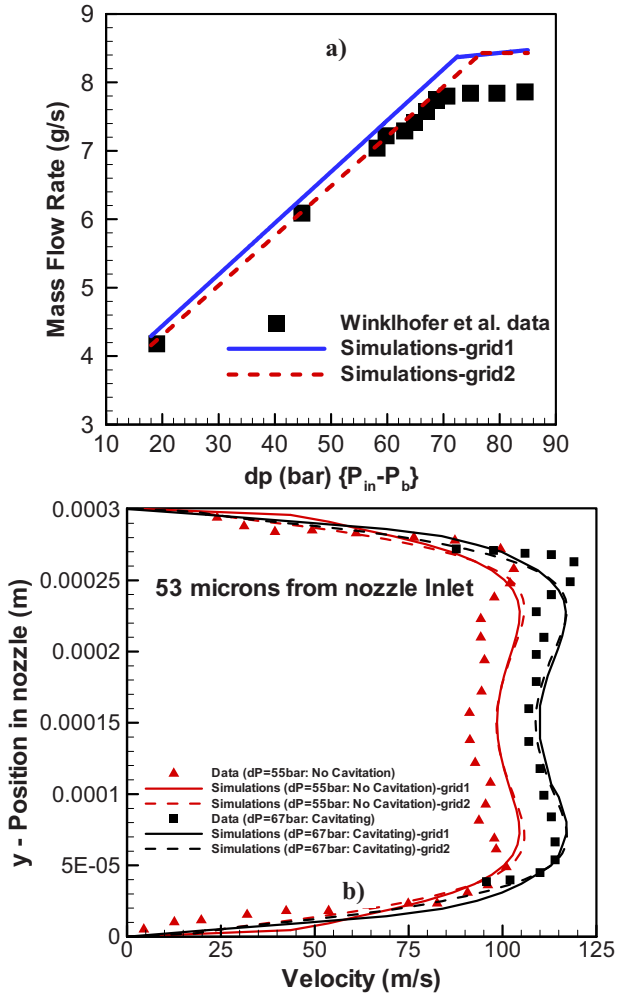

Fig. 2 (*a*) **Predicted (for two different grid densities) and measured (data from Winklhofer et al.) mass flow rates plotted versus the pressure difference (ΔP) (*b*) predicted (for two different grid densities) and measured velocity profiles at a location 53 μm from the nozzle inlet. Simulations are performed at a fixed injection pressure of 100 bar and different back pressures. Grid 1: 90×40; Grid 2: 140×60.**

resentative of orifices in current generation diesel injectors, though the size of the channel is substantially larger than current diesel injector orifices. Fuel temperature was 300 K, and injection pressure was fixed at 100 bar. While this pressure is low for current fuel injection systems, this data set is still useful for validation due to a lack of experimental data under high injection pressure conditions. To reduce the computational time, only the two-dimensional (2D) slice of the rectangular channel flow was considered. The grid-dependency was examined by employing two grid densities in the nozzle block, namely, 90×40 (Grid 1) and 140×60 (Grid 2).

Figure 2(*a*) presents the predicted and measured mass flow rates plotted versus the difference between injection pressure and back pressure (ΔP). Predictions using grid density capture the experimentally observed effect of pressure on mass flow rate, except for some discrepancy in the choked flow region. Simulations predict a higher mass flow rate in this region, which could be due to the 2D assumption in simulations. A 3D flow will offer more resistance, causing a decrease in the mass flow rate. Figure 2(*b*) presents velocity profiles in the transverse direction at a location 53 μm from the nozzle entrance for both cavitating (ΔP =67 bar) and noncavitating (ΔP=55 bar) conditions. The velocity profiles are symmetric about the central plane (y=0.00015), which is expected due to flow symmetry. With higher ΔP, higher velocities are observed. For ΔP=55 bar, the velocity peaks in the shear layer approximately 40 μm from the bottom wall, and then decreases to a minimum value at the center (y=0.00015). Under cavitating conditions (ΔP=67 bar), a similar trend is observed, except that velocities are higher due to larger pressure difference for this case. Simulations capture these trends well except for some overprediction in the nozzle center region. Overall, the finer grid provides a slightly closer agreement with measurements and, hence, is used for further validation.

Figure 3 compares the measured and predicted vapor fraction distributions for three different back pressures and a fixed injection pressure of 100 bar. The experimental images are obtained on a back-lit nozzle with the intensity of transmitted light being proportional to the amount of cavitation. Both experiments and simulations indicate small cavitation regions near the nozzle entrance for P_b=40 bar. With decrease in back pressure, there is significant increase in the amount of cavitation, and simulations capture this behavior well, even though a quantitative comparison could not be done. At P_b=20 bar, both the simulations and experimental images show cavitation patterns extending to the nozzle exit. In summary, the cavitation model in FLUENT is able to capture the inner nozzle flow and cavitation phenomenon well and can therefore be used for comprehensive parametric investigation.

5 Nozzle Flow Characterization

The single orifice simulated for the full-production minisac nozzle used in the present study is shown in Fig. 1. The nozzle has six cylindrical holes with a diameter of 169 μm at an included angle of 126 deg. The discharge coefficient (C_d), velocity coefficient (C_v), and area contraction coefficient (C_a), used to characterize the nozzle flow, are described below. The discharge coefficient (C_d) is calculated from

$$C_d = \frac{M^{\bullet}_{\text{actual}}}{\dot{M}_{\text{th}}} = \frac{M^{\bullet}_{\text{actual}}}{A_{\text{th}}\sqrt{2 * \rho_f * \Delta P}} \tag{12}$$

where $M^{\bullet}_{\text{actual}}$ is the mass flow rate measured by the rate of injection meter [32] or calculated from FLUENT simulations, and A_{th} is the nozzle exit area. The three coefficients are related as [33]

$$C_d = C_v * C_a \tag{13}$$

Here the area contraction coefficient is defined as

$$C_a = \frac{A_{\text{effective}}}{A_{\text{th}}} \tag{14}$$

where $A_{\text{effective}}$ represents the area occupied by the liquid fuel. C_a is an important parameter to characterize cavitation, as it is directly influenced by the amount of vapor present at the nozzle exit. The Reynolds number is calculated from

$$\text{Re} = \frac{V_{\text{th}} D_{\text{th}} \rho_{\text{fuel}}}{\mu_{\text{fuel}}} \tag{15}$$

where D_{th} is the nozzle exit diameter. The cavitation is often characterized in terms of a global cavitation number (CN) defined as

$$CN = \frac{\Delta P}{P_{back} - P_{vapor}} \tag{16}$$

where P_{vapor} represents the fuel vapor pressure at a specific temperature. Properties of different fuels are listed in Table 2. The initial amplitude parameter (A_{mo}) as defined by Li et al. [9] is used to characterize the level of turbulence at the nozzle exit. It is defined as

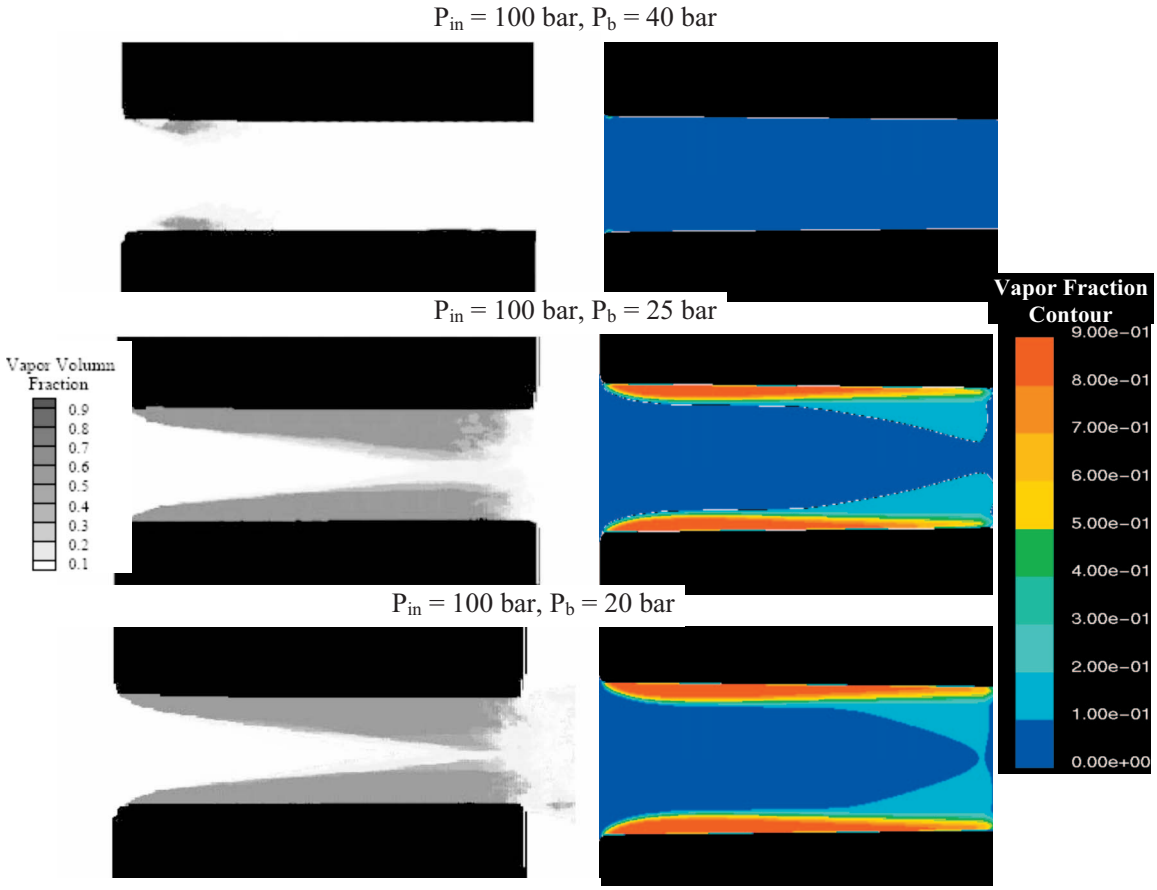

Fig. 3 Comparison between the predicted and measured (data from Winklhofer et al.) vapor fraction contours for three different back pressures and a fixed injection pressure of 100 bar. In simulations the red color indicates the region of high vapor fraction (significant cavitation) while dark blue indicates the region of zero vapor fraction (no cavitation).

$$A_{mo} = \frac{1}{5r\omega_0}\sqrt{\frac{2}{3}k_{\text{avg}}} \tag{17}$$

where r is the nozzle orifice radius, k_{avg} is the average kinetic energy at the orifice exit obtained from the nozzle flow simulations, and ω_0 is the initial droplet oscillation frequency [34] given by

$$\omega_0 = \sqrt{\frac{8\sigma}{\rho_l r^3} - \left(\frac{5\mu_l}{2\rho_l r^2}\right)^2} \tag{18}$$

6 Rate of Injection Measurements

In order to obtain discharge coefficient (C_d) data, ROI experiments are performed at various injection pressures. The ROI was measured using the ROI meter, based on the design described by Bosch [32]. The injector is a hydraulically actuated electronically controlled unit injector (HEUI) 315B. It uses hydraulic pressure from high-pressure oil to increase the fuel pressure to the desired level for direct injection. An internal differential piston multiplies the oil rail pressure with an intensifier ratio of approximately 6.6 to provide high fuel injection pressure. Oil rail pressure was varied from 17 MPa to 24 MPa, while the back pressure was maintained constant at 30 bar for all tests. This was done to simulate the test conditions used in related spray experiments using X-ray radiography at Argonne National Laboratory (ANL) [35]. Typical rate of injection plots obtained are shown in Fig. 4 for the three different rail pressure cases investigated. Following previously described methodology; the actual C_d (cf. Eq. (14)) is then calculated from the measured rate of injection profiles.

Table 2 Fuel properties at 40°C

Property	Viscor/cerium blend	European diesel No. 2	Chevron diesel No. 2	Dodecane
Density (kg/m^3)	865.4	835.0	822.7	745.7
Viscosity (kg/m s)	0.0029	0.0025	0.0021	0.0014
Surface tension (N/m)	0.026	0.020	0.020	0.025
Vapor pressure(Pa)	1057	1000	1000	40

7 Grid-Dependence and Additional Model Validation

The minisac nozzle used in this study is shown schematically in Fig. 1. The computational domain (single orifice) used in the simulations is indicated by a marked box. Assuming the flow to be symmetric across all the nozzle orifices, only a single orifice was simulated at steady state by considering the flow to be two-dimensional. Authors acknowledge that there may be differences between the 3D and 2D flow characteristics, since the throttling area near the orifice inlet is much larger for the 2D case. However, the fact that the mean flow is two-dimensional lends confidence to the 2D approach. In fact, qualitative effects of fuel type, cavitation criterion, etc. will not be affected by the 2D assumption. Also 2D assumption facilitates comprehensive parametric studies, which include in injection pressure range of 2–2400 bar, four different fluids, and several needle lift positions. Such studies would be computationally extremely challenging, if not impossible, with 3D

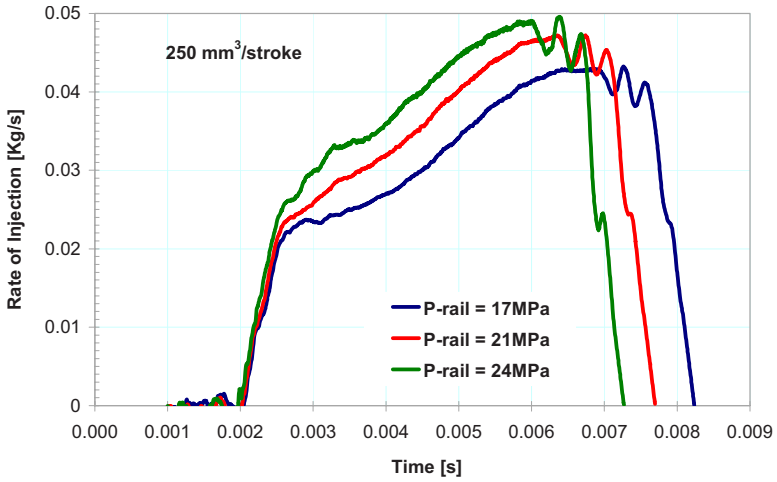

Fig. 4 Rate of injection profiles at different rail pressures

simulations. Moreover, similar two-dimensional studies have been performed previously, providing further justification for our approach [4,30]. Steady state simulations at full needle open position are performed. This may be justified as the flow is expected to be quasisteady during this period since the needle is fully open for approximately 90% of the injection duration [36]. Moreover, estimates of the various time scales indicate that the flow time for a fluid element inside the injection was smaller than the transient time scale. For instance, time for a fluid element to reach the orifice exit is about 40 μs based on an average velocity of 100 m/s and an effective travel length of 4 mm in the longitudinal direction, while the needle transience has a characteristic time of about 0.1 ms for the HEUI injector.

Grid dependence and additional validation studies were performed using the ROI data under quasisteady conditions with the needle full open so that the effects of needle geometry and eccentricity during opening and closing on the internal flow can be isolated. The base grid generated is shown in Fig. 5. A structured mesh was created with a total of 18,040 cells (Grid 1), with 7200 cells (120×60) in the nozzle orifice block itself. A high mesh density is used in the sac region and in the nozzle orifice in order to capture the large pressure and velocity gradients in these regions. The grid refinement studies were performed by increasing the mesh density by factor of 1.5 uniformly, which increased the total number of cells to about 27,000 (Grid 2) with 10,000 cells in the nozzle orifice block. Figure 5 also shows the locations of different boundary conditions imposed, the needle contour, as well as the sac and nozzle orifice regions. The injection and back pressure were varied to simulate different flow conditions.

Using the ROI plots (cf. Fig. 4); discharge coefficients (C_d) were calculated at different rail pressures. It should be noted that the maximum uncertainty in ROI measurement was about 10.5% for the range of range pressures investigated, with a similar level of uncertainty in the C_d values. Simulations were performed using the same surrogate fuel, i.e., Viscor/cerium blend, used in the experiments. Figure 6 presents the measured and computed C_d, corresponding to the full needle open position (0.275 mm), plotted versus rail pressure for the two grids. The correlation of Sarre et al. [41] is also shown. While both simulations and experiments indicate a decrease in flow efficiency with the increase in rail pressure, the decrease is somewhat more significant in experiments. The decrease in C_d is due to the fact that the flow is in the cavitation regime, and as the rail pressure is increased, the amount of cavitation is increased. Simulations with the two grids predict nearly identical C_d values indicating grid independence of the results; consequently Grid 1 (with 18,040 cells) is used for further parametric studies. The correlation of Sarre et al. is based on

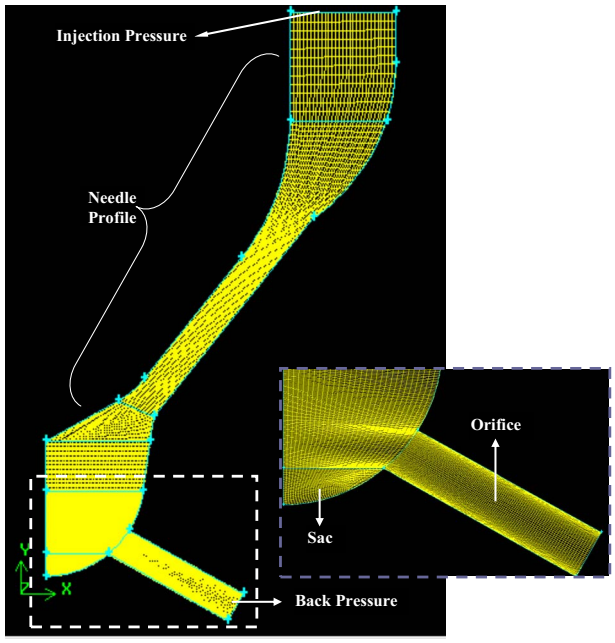

Fig. 5 Grid Generated for cavitation simulations

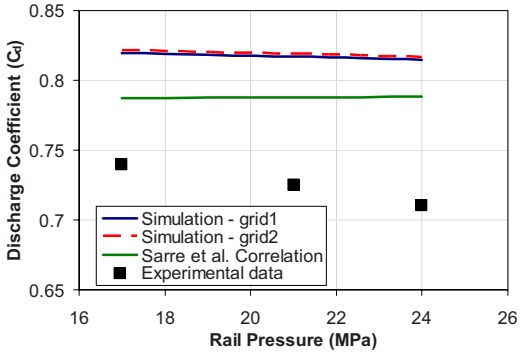

Fig. 6 Predicted (for two different grid sizes) and measured discharge coefficients for different rail pressures. Correlation from Sarre et al. [41] is also shown. Simulations were performed for Viscor/cerium blend with the base nozzle dimensions.

noncavitating conditions, thus, the increase in flow efficiency with rail pressure is not surprising. Another important observation from Fig. 6 is that the simulations overpredict the C_d values at all rail pressures, which may be attributed to fuel leakages that decrease flow efficiency in experiments. Moreover, in a real injector, it is not possible to make pressure measurements inside the nozzle to verify the injection pressure. Therefore, the injection pressure was assumed to be the peak value in simulations. However, it is unknown if the peak injection pressure was ever attained in experiments.

8 An Improved Criterion for Cavitation Inception

According to the traditional criterion, cavitation occurs when the local pressure drops below the vapor pressure of the fuel at a given temperature, i.e., when $-p+p_v>0$. This criterion can be represented in terms of a cavitation index (K) as

$$K_{\text{classical}} = \frac{p - p_b}{p_b - p_v} < -1 \Rightarrow \text{cavitating} \tag{19}$$

where p, p_b, and p_v are the local pressure, back pressure, and vapor pressure, respectively. This criterion has been extensively used in the cavitation modeling community. However, Winer and Bair [37] and Joseph [31] independently proposed that the important parameter for cavitation is the total stress that includes both the pressure and normal viscous stress. This was consistent with the cavitation experiments in creeping shear flow reported by Kottke et al. [38], who observed the appearance of cavitation bubbles at pressures much higher than vapor pressure. Following an approach proposed by Joseph [31] and Dabiri et al. [39], a new criterion based on the principal stresses was derived and implemented in FLUENT simulations. The formulation for the new criterion is summarized below.

For the maximum tension criterion,

$$-p - 2\mu S_{11} + p_v > 0$$

For the minimum tension criterion,

$$-p + 2\mu S_{11} + p_v > 0$$

The new criteria can be expressed in terms of the modified cavitation index as

$$K_{\max} = \frac{p + 2\mu S_{11} - p_b}{p_b - p_v} < -1 \Rightarrow \text{cavitating} \tag{20}$$

$$K_{\min} = \frac{p - 2\mu S_{11} - p_b}{p_b - p_v} < -1 \Rightarrow \text{cavitating} \tag{21}$$

where the strain rate S_{11} is computed as

$$S_{11} = \sqrt{\left(\frac{\partial u}{\partial x}\right)^2 + 0.25\left(\frac{\partial u}{\partial y} + \frac{\partial v}{\partial x}\right)^2} \tag{22}$$

where u and v are the velocities in the x and y directions, respectively.

Under realistic Diesel engine conditions where the flow inside the nozzle is turbulent, turbulent stresses prevail over laminar stresses. Accounting for the effect of turbulent viscosity, the new criterion is further modified as

$$K_{\text{max-turb}} = \frac{p + 2(\mu + \mu_t)S_{11} - p_b}{p_b - p_v} < -1 \Rightarrow \text{cavitating} \tag{23}$$

$$K_{\text{min-turb}} = \frac{p - 2(\mu + \mu_t)S_{11} - p_b}{p_b - p_v} < -1 \Rightarrow \text{cavitating} \tag{24}$$

In order to evaluate this new criterion in realistic diesel injectors, we performed simulations using the nozzle described earlier (cf. Fig. 1). To the best of our knowledge, this is the first time that this new criterion has been evaluated under realistic diesel engine conditions. Previously such criteria have been examined under laminar conditions in simplified geometries [40]. Simulations were performed for a peak injection pressure of 1367 bar and an injection pressure of 100 bar with a constant back pressure of 1 bar at the full needle open position. Figures 7 and 8 present K contours computed using the traditional criterion based on local pressure, as well as the new criteria based on the minimum and maximum total stresses incorporating the effects of molecular and turbulent viscosity. Note for all these criteria, the cavitation region is characterized by K less than -1.

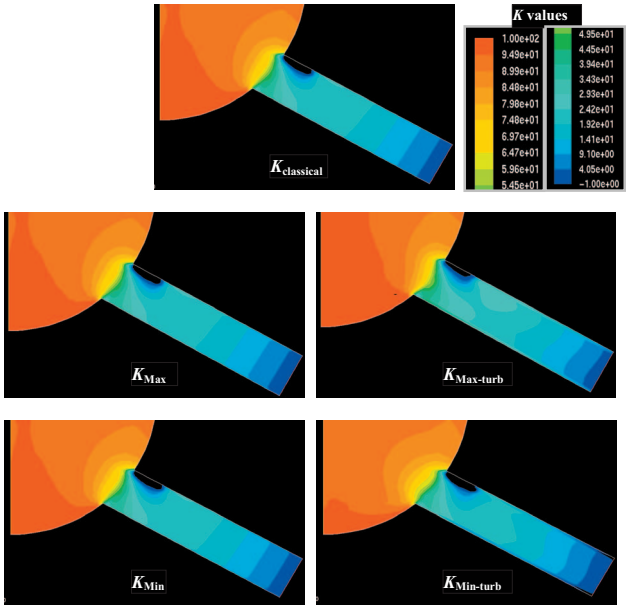

Fig. 7 *K* contours computed for injection pressure of 100 bar and back pressure of 1 bar using the different cavitation inception criteria for the nozzle orifice described in Fig. 5. Only the nozzle orifice and sac regions are shown.

As expected, K contours based on the classical criterion (cf. Figs. 7 and 8) coincide with vapor fraction contours (not shown),

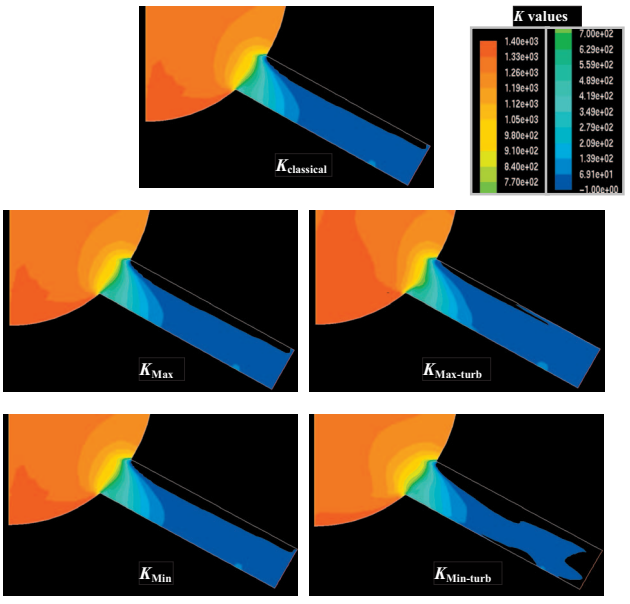

Fig. 8 *K* contours computed for injection pressure of 1367 bar and back pressure of 1 bar using the different cavitation inception criteria for the nozzle orifice described in Fig. 5. Only the nozzle orifice and sac regions are shown.

indicating that the cavitation index can be used to determine the vapor fraction distribution at the orifice exit. Cavitation criteria based on molecular viscosity (K_{max}, K_{min}) show negligible difference with the classical criterion for both injection pressures. In fact, the average K values at the nozzle exit do not show any difference between the three criteria ($K_{classical}, K_{max}, K_{min}$). Since spray development outside the nozzle depends on the average vapor fraction at the nozzle exit, it is not expected to be modified significantly using the new criteria based on molecular viscosity. These results are consistent with those of Dabiri et al. [39], who reported that the differences between the criteria in terms of the possible cavitation regions become less significant at high Reynolds numbers (i.e., at high injection pressures).

Incorporating the criteria based on turbulent viscosity at an injection pressure of 100 bar (cf. Fig. 7), minor differences are observed between the maximum tension ($K_{max\text{-}turb}$) and minimum tension criteria ($K_{min\text{-}turb}$). The minimum tension criterion indicates marginally larger cavitation pockets. However, this minimum tension criterion is a necessary but not sufficient condition, implying the possibility for cavitation inception. In contrast, K contours corresponding to the maximum tension criterion ($K_{max\text{-}turb}$) indicate marginally reduced cavitation pockets compared with those for the traditional criterion. The differences among these turbulent viscosity based criteria become more pronounced at high injection pressures (cf. Fig. 8). While the minimum tension criterion predicts significantly larger cavitation pockets, the maximum tension criterion shows smaller pure vapor regions. Thus, an important observation here is that under realistic high-pressure diesel engine conditions, the turbulent viscosity based criteria for cavitation inception modifies the vapor fraction distribution inside the nozzle. This can be explained by the fact that while molecular viscosity is independent of the Reynolds number, turbulent viscosity increases as the injection pressure or Reynolds number is increased. Cavitation experiments under realistic diesel engine conditions (high injection and back pressures) with real injectors (not scaled up) are necessary for validating such criteria. Unfortunately, according to the best of our knowledge, such quantitative information is missing for production nozzles, which inhibits a detailed evaluation of these criteria.

9 Effect of Injection Pressure

During an injection event, the injection pressure generally ramps up reaching a peak value. In typical diesel engines, the injection pressure can vary from few hundred bars to peak values of 2500 bar or more and, therefore, it is important to examine the internal nozzle flow characteristics over this wide pressure range. Simulations were performed by varying the injection pressure from 2 bar to 2400 bar at a fixed back pressure of 1 bar. Figure 9(a) presents the discharge coefficient and initial amplitude parameter plotted versus the Reynolds number for European diesel fuel No. 2 at full open needle (0.275 mm) condition. Three distinct flow regimes are observed, namely, the laminar regime where the discharge coefficient varies as square root of the Reynolds number (Re), the turbulent regime where the discharge coefficient is nearly independent of Re, and the cavitation regime where the discharge coefficient decreases, albeit slightly, with Re. Similar flow regimes have been observed by Sarre et al. [41]. The decrease in C_d in the cavitation regime is expected, as the amount of fuel vapor in the exit stream increases as the injection pressure is increased. This aspect is further discussed in Sec. 11. The initial amplitude parameter increases linearly with the Reynolds number indicating higher turbulence levels at nozzle exit as the injection pressure is increased. These results clearly suggest that the primary breakup model should account for the effects of cavitation and turbulence, in addition to the aerodynamic effect.

Figure 9(b) presents the variation in discharge coefficient (C_d) and area contraction coefficient (C_a) with Re in the turbulent and cavitation regimes. Clearly, prior to the cavitation regime, the exit

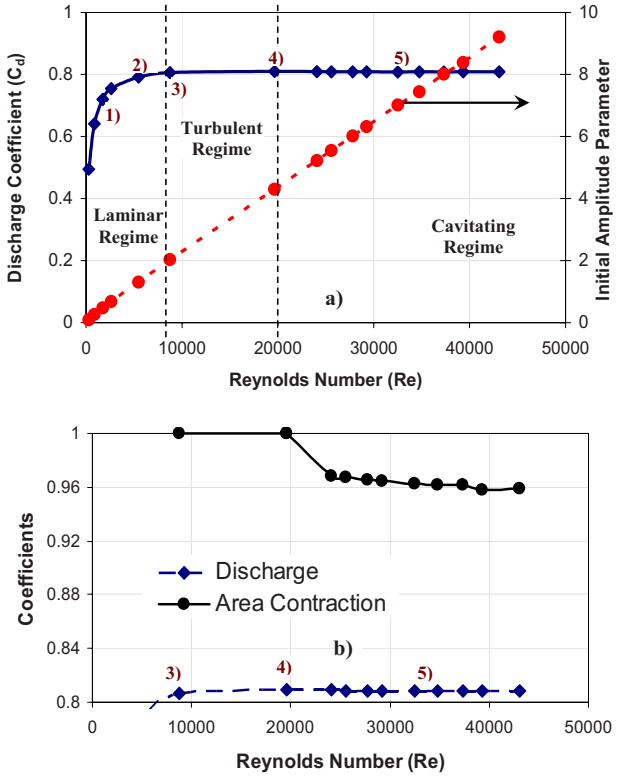

Fig. 9 (a) Discharge coefficient and initial amplitude parameter plotted versus the Reynolds number for different flow regimes, (b) discharge (C_d), and area contraction (C_a) coefficients plotted versus the Reynolds number in the turbulent and cavitation flow regimes. Simulations were performed at full needle open position for European diesel No. 2 fuel, base nozzle dimensions, and a fixed back pressure of 1 bar.

stream is purely liquid and $C_a=1$. As the injection pressure is increased, the cavitation patterns generated at the orifice entrance advect and reach the nozzle exit, and both C_d and C_a decrease in the cavitation regime. For the present nozzle, this occurs at Re $=20,000$ corresponding to $P_{in}=500$ bar and $P_b=1$ bar. Further increase in injection pressure (or Re) only causes a slight decrease in C_d and C_a.

Figure 10 presents vapor fraction contours at different injection pressures corresponding to different points in Fig. 9. Cavitation inception is first observed at the orifice inlet for an injection pressure of 40 bar (cf. Fig. 10.2). Increasing the injection pressure to 100 bar causes a slight increase in flow efficiency or discharge coefficient (C_d). This pressure corresponds to the turbulent regime in which C_d is nearly independent of Re. Further increase in injection pressure causes increasing levels of cavitation, and eventually the cavitation patterns reach the nozzle exit (cf. Fig. 10.4), causing a decrease in C_d, as discussed earlier. However, a further increase in injection pressure does not change the cavitation structure significantly (cf. Fig. 10.5).

10 Effect of Different Fuels on Cavitation and Nozzle Exit Parameters

Simulations were performed for four different fluids in order to examine the effects of fuel type on the cavitation characteristics. The fuels include the two on-fleet diesel fuels (Chevron diesel fuel No. 2 and European diesel fuel No. 2), a surrogate for diesel fuel (n-dodecane) and a Viscor/cerium blend that has been extensively used as a surrogate for spray studies at Argonne National Laboratory [42]. The relevant properties of these fuels are listed in Table 2. Simulations were performed by varying the injection pressure

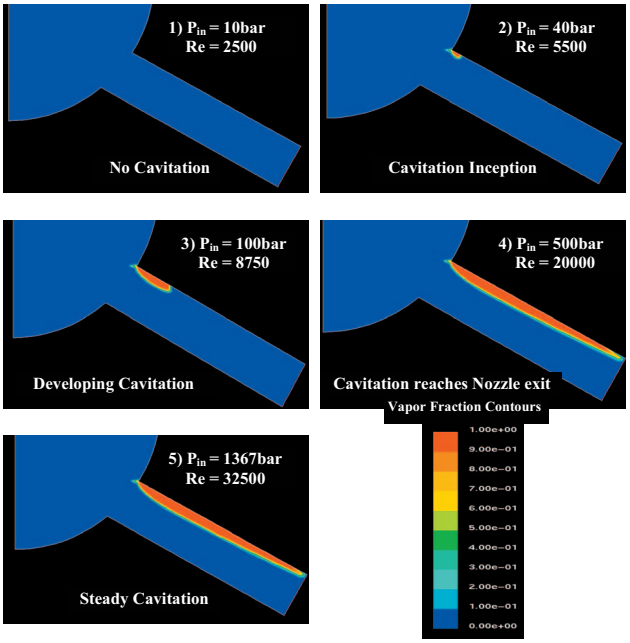

Fig. 10 Cavitation (vapor fraction) contours for different injection pressures used in the context of Fig. 9, and a fixed back pressure of 1 bar. Simulations were performed with base nozzle dimensions for European diesel No. 2 fuel.

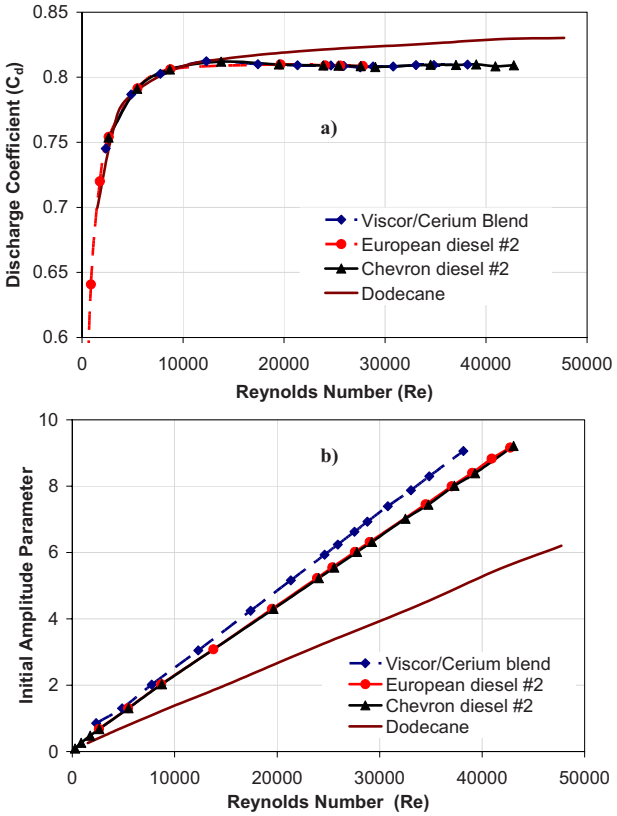

Fig. 11 (*a*) Discharge coefficient and (*b*) initial amplitude parameter plotted versus Re for different fuels at full needle open position (0.275 mm) with base nozzle dimensions. Simulations were performed by varying the injection pressure at a fixed back pressure of 1 bar.

with needle at full open position (0.275 mm) and a fixed back pressure (P_b) of 1 bar. It should be noted that the effects of fuel on cavitation characteristics and discharge coefficient are not expected to be significantly different as the back pressure changes from 1 bar to 30 bar, since the effect of back pressure has been shown to be negligible [9].

Figure 11 presents the discharge coefficient and initial amplitude parameter plotted versus Re for different fuels. For all three flow regimes discussed in the context of Fig. 9, the variation in C_d and initial amplitude parameter with the Reynolds number is essentially the same for Viscor/cerium blend, European diesel No. 2 and Chevron diesel No. 2. This can be expected since there are no significant differences between the vapor pressures (as well as other properties) of these fluids. Consequently, for these three fluids, the cavitation inception occurs nearly at the same Reynolds number (or injection pressure), and the cavitation regime is characterized by the same range of Reynolds numbers (or injection pressures). There are, however, significant differences between the predicted nozzle flow characteristics for n-dodecane and other three fluids. The predicted C_d for n-dodecane is higher than that for the other three fluids in the turbulent regime, which is due to the fact that the propensity to cavitation (cf. Fig. 13), as well as viscous losses, are lower for the fuel surrogate (cf. Table 2). As indicated in Fig. 11(*b*), the initial amplitude parameter for n-dodecane is significantly lower compared with that for the other fluids, implying significantly lower level of turbulence at the nozzle exit.

At a given injection pressure, the Reynolds number can vary for different fuels due to the difference in their properties. In order to isolate this effect, we plot in Fig. 12 the discharge coefficient versus the cavitation number (*CN*) for the four fuels. As discussed earlier, *CN* represents the normalized pressure difference and may be more relevant to characterize the fuel vapor pressure effects. The variation of C_d with CN for the four fuels is qualitatively similar to that of C_d with Re (cf. Fig. 11(*a*)) implying that the effect of fuel may be predominantly due to its viscosity and vapor pressure.

Figure 13 presents vapor fraction contours and pressure contours inside the nozzle for three different fluids at P_{in}=1000 bar and P_b=1 bar. Results for Chevron diesel No. 2 are not shown, since its flow characteristics are similar to those of European diesel No. 2. The vapor fraction contours indicate relatively little cavitation for n-dodecane compared with that for other two fluids. For n-dodecane, there is a small cavitation region near the orifice inlet, while for the other two fluids, the vapor fraction contours extend up to the orifice exit, and this behavior is directly attributable to the low vapor pressure of n-dodecane. Pressure distribution also reveals a narrow low pressure region near the orifice

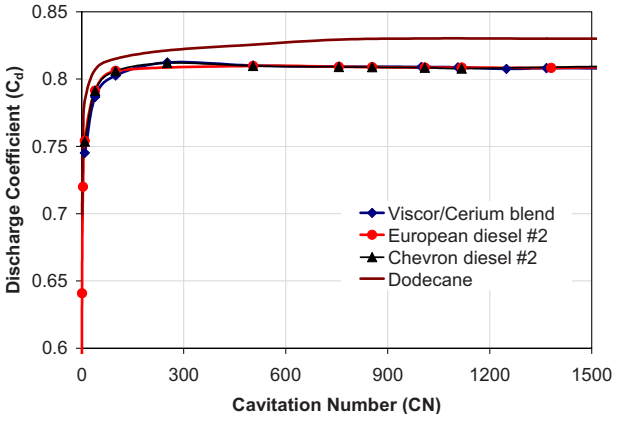

Fig. 12 Discharge coefficient plotted versus the cavitation number for different fuels at full needle open position (0.275 mm) with base nozzle dimensions. Simulations were performed by varying the injection pressure and a fixed back pressure of 1 bar.

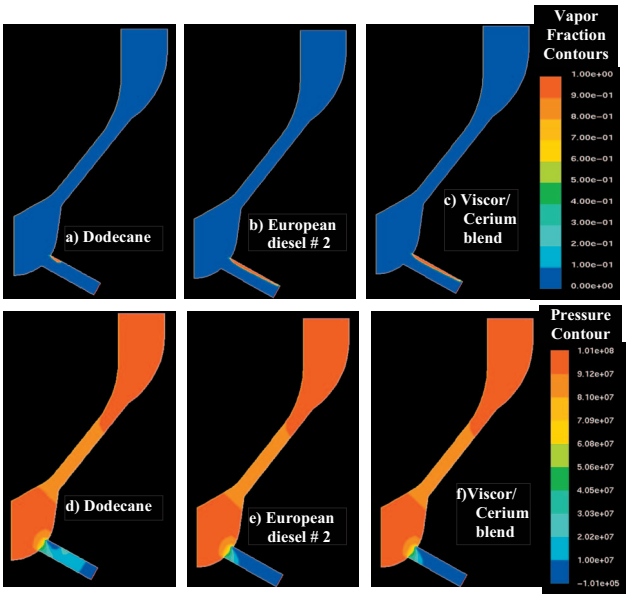

Fig. 13 Vapor fraction contours (top three) for n-dodecane (*a*), European diesel No. 2 (*b*), Viscor/cerium blend (*c*), and pressure contours (bottom three) for n-dodecane (*d*), European diesel No. 2 (e), and Viscor/cerium blend (f) at $P_{in}=1000$ bar, $P_b=1$ bar at full needle open position (0.275 mm)

Table 3 Base nozzle orifice characteristics

Nozzle type	Minisac
Nozzle exit diameter	169 μm
Length to diameter ratio	4.2
K -factor	0
r/R ratio	0
Maximum needle lift	0.275 mm

inlet for dodecane. In summary, the flow and cavitation characteristics of n-dodecane (a surrogate for diesel fuel) are noticeably different from those of the other three fuels investigated. In particular, for n-dodecane, the flow losses are lower and thus the flow efficiency is higher, while the turbulence levels and vapor fractions are lower compared with those for the other three fuels, implying relatively poor spray breakup and atomization characteristics for the former.

11 Effect of Needle Lift on Cavitation and Nozzle Characteristics

The injection event is inherently transient, as the injection pressure varies with the needle lift position. The peak needle lift position for the HEUI 315B injector is 0.275 mm. In order to capture this transient aspect within a steady-state formulation, we performed simulations for different lift positions for the base nozzle (cf. Table 3) at a back pressure of $P_b=30$ bar. The injection pressure was assumed to vary linearly with needle lift. For instance, $P_{in}=1367$ bar at full needle open position (0.275 mm) and $P_{in}=683.5$ bar at half needle open position. Figure 14 presents the vapor fraction distribution (cf. Figs. 14(*a*)–14(*e*)) for needle lift positions at 0.275 mm, 0.2 mm, 0.15 mm, 0.1 mm, and 0.05 mm. Simulations are able to capture the transient flow behavior, as the amount of cavitation and the location of cavitation region change significantly with the needle lift position. For full needle open position, the cavitation occurs near the top portion of the orifice. As the needle moves down (needle lift=0.2 mm), the cavitation region is reduced, and for needle lift=0.15 mm, there is essentially no cavitation. Subsequently, with needle lift position at 0.1 mm, cavitation occurs in the lower part of the orifice, while with needle lift position at 0.05 mm, there is again no cavitation region. To the best of our knowledge such shift in cavitation patterns has not been observed by any previous numerical investigation, although an experimental evidence of this shift in VCO nozzles has been reported [43].

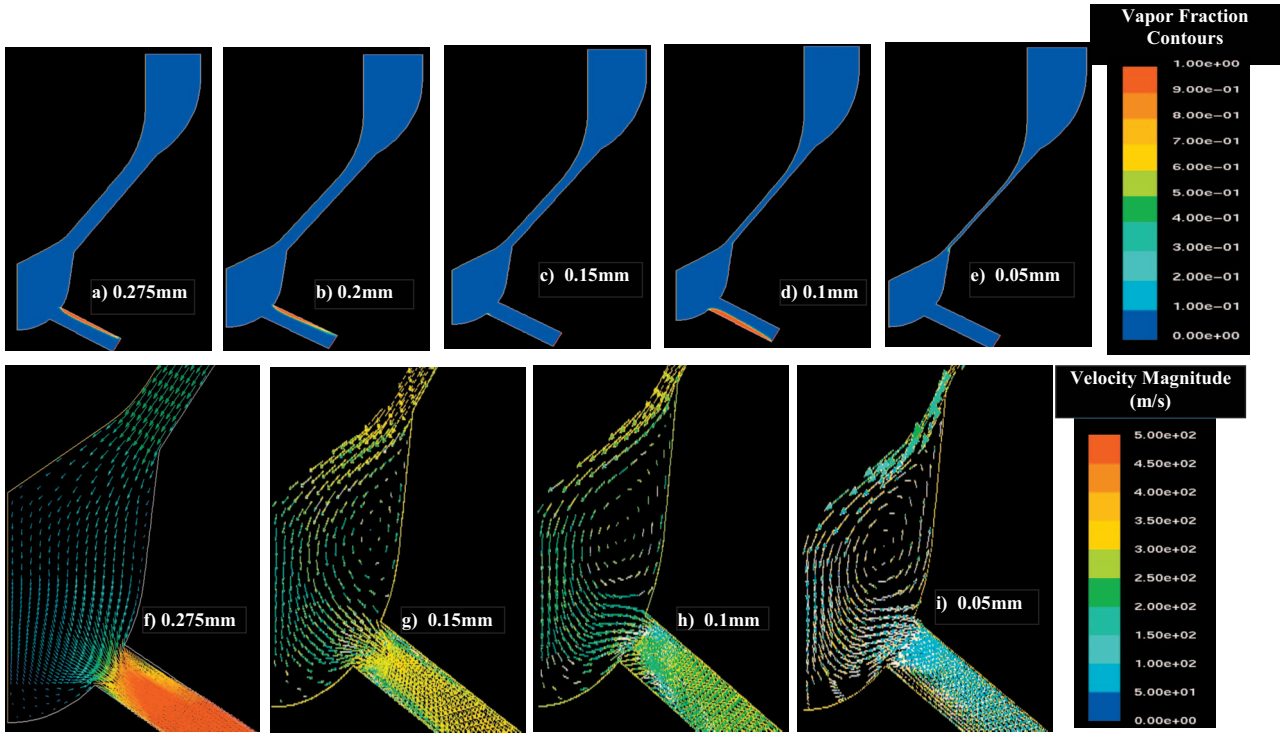

Fig. 14 Vapor fraction contours (top five) at different needle lift positions: (*a*) 0.275 mm (fully open), (*b*) 0.2 mm, (*c*) 0.15 mm, (*d*) 0.1 mm, and (*e*) 0.05 mm. Velocity vectors (bottom four) at different needle lift positions: (*f*) 0.275 mm (fully open), (*g*) 0.15 mm, (*h*) 0.1 mm, and (*i*) 0.05 mm. Simulations were performed with base nozzle and Viscor/cerium liquid blend at $P_b=30$ bar.

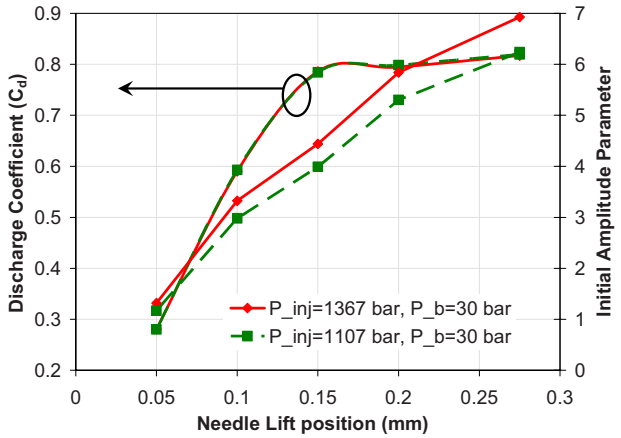

Fig. 15 Discharge coefficient and initial amplitude parameter plotted versus needle lift position, as discussed in context of Fig. 14, for two peak injection pressures. Simulations were performed for the Viscor/cerium blend with the base nozzle orifice dimensions.

In order to explain the transient cavitation behavior, we present in Fig. 14 the corresponding velocity vector plots (cf. Figs. 14(*f*)–14(*i*)) for different needle lift positions. The velocity vectors for needle lift=0.2 mm are not shown as these were quite similar to those of 0.275 mm needle lift position. The velocity vectors for the full needle open position (cf. Fig. 14(*f*)) indicate that the flow entering the orifice encounters a sharp bend (i.e., large velocity and pressure gradients) at the top of the orifice inlet causing cavitation in this region, as indicated by the vapor fraction contours in Fig. 14(*a*). However, with needle lift position at 0.15 mm, the flow entrance into the orifice is relatively smooth. This is due to the fact that the flow is restricted between the needle and nozzle wall, and a sudden expansion results in a recirculation zone downstream of the restriction. This causes the velocity vectors to be aligned in a manner that the entry to the nozzle orifice is smooth thus inhibiting cavitation (cf. Figs. 14(*c*) and 14(*g*)). Farther downward movement of the needle (needle lift=0.1 mm) results in a stronger recirculation zone. The velocity vectors are aligned such that the entry at the orifice top is smooth, but the entry at the orifice bottom is sharp causing cavitation in the bottom region (cf. Figs. 14(*d*) and 14(*h*)). At needle lift=0.05, although the velocity vectors encounter a sharp bend, the gradients are not sufficiently large to cause cavitation (cf. Figs. 14(*e*) and 14(*i*)), since the injection pressure is too low for cavitation. Similar transient nature of cavitation phenomenon has been reported by Li et al. [9].

Figure 15 presents the global nozzle characteristics in terms of discharge coefficient and initial amplitude parameter plotted versus the needle lift position for the cases discussed in the context of Figs. 14 and 15. Results are shown for two peak injection pressures (corresponding to rail pressures of 17 MPa and 21 MPa), which correspond to the full open needle position, and indicate that C_d is essentially independent of the peak injection pressure, irrespective of the needle lift position. This is consistent with the results discussed earlier in the context of Fig. 9. The amplitude parameter is higher value for the higher injection pressure case, which is expected, since an increase in injection pressure leads to higher turbulence level.

12 Conclusions

We have reported a comprehensive investigation of internal nozzle flow characteristics and cavitation phenomenon inside a single orifice of HEUI 315B diesel injector. The mixture approach based model in FLUENT V6.2 software has been employed. In addition, a new criterion for cavitation inception based on the total stress has been implemented, and its effectiveness in predicting cavitation has been evaluated under realistic diesel engine conditions. Simulations have been validated using the available two-phase nozzle flow data and the ROI measurements from the present study. The computational model has been used to characterize the effects of important injector parameters on the internal nozzle flow and cavitation behavior and on flow properties at the nozzle exit. These parameters include injection pressure, needle lift position, and fuel type. The major conclusions are as follows.

1. The cavitation model in FLUENT was able to predict all the experimental trends reported in the literature and also matched quantitatively with the data of Winklhofer et al.
2. Simulations with the new cavitation criterion, which is based on the total stress, indicated significant regions of cavitation inception under realistic diesel injection conditions. This suggests the need for cavitation experiments under diesel engine conditions for a detailed evaluation of this criterion.
3. Cavitation characteristics of the two on-fleet fuels (Chevron diesel No. 2 and European diesel No. 2) and a Viscor/cerium blend (surrogate fluid) are quite similar. There are noticeable differences, however, between the cavitation characteristics of these three fuels and n-dodecane (a surrogate for diesel fuel). The cavitation and turbulence levels at nozzle exit are lower, while the nozzle flow efficiency (or discharge coefficient) is higher for n-dodecane compared with those for the other three fuels.
4. The effect of needle movement on cavitation has been investigated by performing simulations at different needle lift positions. Cavitation patterns are seen to shift dramatically as the needle lift position is changed during an injection event. The region of significant cavitation shifts from top of the orifice to bottom of the orifice as the needle position is changed from fully open (0.275 mm) to 0.1 mm. The behavior can be attributed to the effect of needle position on flow patterns upstream of the orifice. Such shift in cavitation patterns has not been observed in previous numerical investigations, although an experimental evidence of this shift in VCO nozzles has been reported

Acknowledgment

This work has been supported by the U.S. Department of Energy Office of Vehicle Technology under the management of Gurpreet Singh. Many useful discussions with Dr. Chris Powell and Dr. Alan Kastengren at Argonne National Laboratory are greatly appreciated. The submitted manuscript has been created by UChicago Argonne, LLC, Operator of Argonne National Laboratory ("Argonne"). Argonne, a U.S. Department of Energy Office of Science laboratory, is operated under Contract No. DE-AC02-06CH11357.

References

[1] Franc, J. P., Avellan, F., Bela-Hadji, B., Billard, J. Y., Briancon-Marjollet, L., Frechou, D., Fruman, D. H., Karimi, A., Kueny, J. L., and Michel, J. M., 1995, *La Cavitation*, Presses Universitaries de Grenoble, Collection Grenoble Sciences, France.
[2] Han, J. S., Lu, P. H., Xie, X. B., Lai, M. C., and Henein, N. A., 2002, "Investigation of Diesel Spray Break Up and Development for Different Nozzle Geometries," SAE Paper No. 2002-01-2775.
[3] Giannadakis, E., 2005, "Modeling of Cavitation in Automotive Fuel Injector Nozzles," Ph.D. thesis, Imperial College, London.
[4] Schmidt, D. P., Rutland, C. J., Corrandini, M. L., Roosen, P., and Genge, O., 1999, "Cavitation in 2-D Asymmetric Nozzles," SAE Paper No. 1999-01-0518.
[5] Wallis, G. B., 1969, *One-Dimensional Two-Phase Flow*, McGraw-Hill, New York.
[6] Avva, R. K., Singhal, A., and Gibson, D. H., 1995, "An Enthalpy Based Model of Cavitation," ASME J. Fluids Eng., **226**, pp. 63–70.
[7] Habchi, C., Dumont, N., and Simonin, O., 2003, "CAVIF: A 3D Code for the Modeling of Cavitating Flows in Diesel Injectors," ICLASS Sorrento 2003, Paper No. 95.
[8] Ning, W., Reitz, R. D., Diwakar, R., and Lippert, A. M., 2008, "A Numerical Investigation of Nozzle Geometry and Injection Condition Effects on Diesel Fuel Injector Flow Physics," SAE Paper No. 2008-01-0936.

[9] Li, M., Mulemane, A., Lai, M. C., and Poola, R., 2005, "Simulating Diesel Injectors Based on Different Cavitation Modeling Approaches," ASME Paper No. ICES2005-1030.
[10] Chen, Y., and Heister, S. D., 1995, "Two-Phase Modeling of Cavitated Flows," Comput. Fluids, **24**, pp. 799–806.
[11] Martynov, S., 2005, "Numerical Simulation of Cavitation Process in Diesel Fuel Injectors," Ph.D. thesis, University of Brighton, Brighton.
[12] Singhal, A. K., Athavale, M. M., Li, H., and Jiang, Y., 2002, "Mathematical Basis and Validation of the Full Cavitation Model," ASME J. Fluids Eng., **124**, pp. 617–624.
[13] Tatschl, R., Sarre, C. V. K., Alajbegovic, A., and Winklhofer, E., 2000, "Diesel Spray Break-Up Modeling Including Multi-Dimensional Cavitating Nozzle Flow Effects," 16th ILASS Conference-Europe.
[14] Chiavola, O., Palmieri, F., 2006, "Coupling Codes for Nozzle Flow Modeling in Diesel Injection System," ASME Paper No. ICES2006-1414.
[15] Dirke, M. V., Krautter, A., Ostertag, J., Mennicken, M., and Badock, C., 1999, "Simulation of Cavitating Flows in Diesel Injectors," Oil Gas Sci. Technol., **54**, pp. 223–226.
[16] Giannadakis, E., Gavaises, M., Roth, H., and Arcoumanis, C., 2004, "Cavitation Modeling in Single-Hole Diesel Injector Based on Eulerian-Lagrangian Approach," *Proceedings of the THIESEL International Conference on Thermo- and Fluid Dynamic Process in Diesel Engines*, Valencia, Spain.
[17] Winklhofer, E., Kull, E., Kelz, E., and Morozov, A., 2001, "Comprehensive Hydraulic and Flow Field Documentation in Model Throttle Experiments Under Cavitation Conditions," ILASS Europe 2001.
[18] Payri, R., Margot, X., and Salvador, F. J., 2002, "A Numerical Study of the Influence of Diesel Nozzle Geometry on the Inner Cavitating Flow," SAE Paper No. 2002-01-0215.
[19] Soteriou, C., and Andrews, R., 1998, "Diesel Injection-Laser Light Sheet Illumination of the Development of Cavitation in Orifices," IMechE Conf. Trans., **C529**(018), pp. 137–158.
[20] Arcoumanis, C., Flora, H., Gavaises, M., and Badami, M., 2000, "Cavitation in Real-Size Multi-Hole Diesel Injector Nozzles," SAE Paper No. 2000-01-1249.
[21] Roth, H., Giannadakis, E., Gavaises, M., Arcoumanis, C., Omae, K., Sakata, I., Nakamura, M., and Yanagihara, H., 2005, "Effect of Multi-Injection Strategy on Cavitation Development in Diesel Injector Nozzle Holes," SAE Paper No. 2005-01-1237.
[22] Benajes, J., Pastor, J. V., Payri, R., and Plazas, A. H., 2004, "Analysis of the Influence of Diesel Nozzle Geometry in the Injection Rate Characteristics," ASME J. Fluids Eng., **126**, pp. 63–71.
[23] Badock, C., Wirth, R., Fath, A., and Leipertz, A., 1999, "Investigation of Cavitation in Real Size Diesel Injection Nozzles," Int. J. Heat Fluid Flow, **20**, pp. 538–544.
[24] Chaves, H., Knapp, M., and Kubitezek, A., 1995, "Experimental Study of Cavitation in the Nozzle Hole of Diesel Injectors Using Transparent Nozzles," SAE Paper No. 950290.
[25] Payri, F., Bermudez, V., Payri, R., and Salvador, F. J., 2004, "The Influence of Cavitation on the Internal Flow and the Spray Characteristics in Diesel Injection Nozzles," Fuel, **83**, pp. 419–431.
[26] Ning, W., Reitz, R. D., Diwakar, R., and Lippert, A. M., 2007, "Development of a Next Generation Spray and Atomization Model Using an Eulerian-Lagrangian Methodology," 20th ILASS Americas 2007.
[27] Ibrahim, A. A., and Jog, M. A., 2007, "Nonlinear Breakup Model for a Liquid Sheet Emanating From a Pressure-Swirl Atomizer," ASME J. Eng. Gas Turbines Power, **129**, pp. 945–953.
[28] Gavaises, M., and Arcoumanis, C., 2001, "Modeling of Sprays From High-Pressure Swirl Atomizers," Int. J. Engine Res., **2**(2), pp. 95–117.
[29] FLUENT V6.2 Documentation.
[30] Jia, M., Hou, D., Li, J., Xie, M., and Liu, H., 2007, "A Micro-Variable Circular Orifice Fuel Injector for HCCI-Conventional Engine Combustion-Part 1 Numerical Simulation of Cavitation," SAE Paper No. 2007-01-0249.
[31] Joseph, D. D., 1998, "Cavitation and the State of Stress in a Flowing Liquid," J. Fluid Mech., **366**, pp. 367–378.
[32] Bosch, W., 1966, "The Fuel Rate Indicator: A New Measuring Instrument for Display of the Characteristics of Individual Injection," SAE Paper No. 660749.
[33] Naber, J. D., and Siebers, D. L., 1996, "Effects of Gas Density and Vaporization on Penetration and Dispersion of Diesel Sprays," SAE Paper No. 960034.
[34] O'Rourke, P. J., and Amsden, A. A., 1987, "The TAB Method for Numerical Calculation of Spray Droplet Breakup," SAE Paper No. 872089.
[35] Ramirez, A. I., Som, S., Aggarwal, S. K., Kastengren, A. L., El-Hannouny, E., Longman, D. E., and Powell, C. F., 2008, "Quantitative Measurement of Diesel Fuel Spray Characteristics in the Near-Nozzle Region of a Heavy Duty Multi-Hole Injector," 21st ILASS Americas 2008.
[36] Mulemane, A., Han J. S., Lu, P. H., Yoon, S. J., and Lai, M. C., 2004, "Modeling Dynamic Behavior of Diesel Fuel Injection Systems," SAE Paper No. 2004-01-0536.
[37] Winer, W. O., and Bair, S., 1987, "The Influence of Ambient Pressure on the Apparent Shear Thinning of Liquid Lubricants—an Overlooked Phenomenon," Proceedings of the Institute of Mechanical Engineers—Tribology 50 Years On, Paper No. 190/187, pp. 395–398.
[38] Kottke, P. A., Bair, S. S., and Winer, W. O., 2005, "Cavitation in Creeping Shear Flows," AIChE J., **51**, pp. 2150–2170.
[39] Dabiri, S., Sirignano, W. A., and Joseph, D. D., 2007, "Cavitation in an Orifice Flow," Phys. Fluids, **19**, p. 072112.
[40] Padrino, J. C., Joseph, D. D., Funada, T., Wang, J., and Sirignano, W. A., 2007, "Stress-Induced Cavitation for the Streaming Motion of a Viscous Liquid Past a Sphere," J. Fluid Mech., **578**, pp. 381–411.
[41] Sarre, C. V. K., Kong, S. C., and Reitz, R. D., 1999, "Modeling the Effects of Injector Nozzle Geometry on Diesel Sprays," SAE Paper No. 1999-01-0912.
[42] Kastengren, A. L., and Powell, C. F., 2007, "Spray Density Measurements Using X-Ray Radiography," Proc. Inst. Mech. Eng., Part D (J. Automob. Eng.), **221**, pp. 653–662.
[43] Bittlinger, G., Henle, A., Hertlein, D., Leick, P., and Kunz, T., 2006, "Optische Methoden zur Bewertung der dieselmotorischen Gemischbildung und Verbrennung," Fifth Conference on Diesel and Gasoline Direct Injection, Berlin, Germany.